CARBON 48 (2010) 3057–3065

available at www.sciencedirect.com

ScienceDirect

journal homepage: www.elsevier.com/locate/carbon

Nitrogen doped carbon nanotubes and their impact on the oxygen reduction reaction in fuel cells

Zhu Chen, Drew Higgins, Zhongwei Chen *

Department of Chemical Engineering, Waterloo Institute of Nanotechnology, Waterloo Institute for Sustainable Energy, University of Waterloo, Waterloo, Ontario, Canada N2L 3G1

ARTICLE INFO

Article history:
Received 28 October 2009
Accepted 22 April 2010
Available online 28 April 2010

ABSTRACT

Nitrogen doped carbon nanotubes (N-CNTs) with different nitrogen contents were synthesized as non-precious catalysts for oxygen reduction reaction (ORR) through varying the relative amount of pyridine and ethanol in the stock solution. The structural and chemical properties of the N-CNTs were investigated using scanning electron microscopy, transmission electron microscopy and X-ray photoelectron spectroscopy. The characterizations indicated that an increase in the pyridine to ethanol ratio of the stock solution produced N-CNTs with higher nitrogen contents. The electrocatalytic activity of N-CNTs towards ORR in alkaline conditions was evaluated using rotating ring disc electrode voltammetry which showed a positive correlation between nitrogen content and ORR activities. By combining the results of ORR activity and material characterization, it is concluded that an increase in the nitrogen content of N-CNTs can effectively improve the ORR activities.

1. Introduction

Low temperature fuel cells are a promising energy conversion technology due to their high efficiency and low emissions [1–3]. An important area of application of CNTs in low temperature fuel cells is towards the oxygen reduction reaction (ORR) taking place on the fuel cell cathode. Currently, platinum based materials are used as catalyst for ORR on fuel cell cathodes. However, due to the scarcity, high cost and sluggish ORR kinetics of platinum based catalysts, large scale commercialization of fuel cells cannot be realized [1–3]. Developing inexpensive electrocatalysts with high ORR activities will significantly accelerate the process of fuel cell commercialization [1–3].

Carbon nanotubes (CNTs) have been investigated for a wide range of applications, including composite materials [4,5], molecular sensing [6–10], energy conversion and energy storage [11–15], due to their unique structures and excellent properties [16–20]. Recently CNTs have been utilized as catalyst supports to reduce Pt loading and improve long-term stability due to their chemical stability and high surface area [21,22]. However, the inherently low ORR activity of pristine CNTs limits the application as electrocatalysts [23]. Thus, improving the ORR activity of CNTs can produce an inexpensive electrocatalyst possessing high surface area and chemical stability while eliminating the need for an inert electrocatalyst support. From previous studies, carbon materials containing nitrogen atoms have been studied and shown to have significantly improved ORR activities [24,25]. Based on modelling results, addition of nitrogen atoms to the graphitic network of pristine CNTs has been predicted to improve the surface chemical reactivity of the materials. More importantly, the electron donation process from carbon to oxygen can be facilitated by the extra electrons introduced into the graphite network through doping which leads to enhanced ORR activity [26,27]. Higher ORR activities compared to pristine CNTs were displayed by nitrogen doped carbon nanotubes (N-CNTs) synthesized using chemical vapour deposition (CVD) technique [28–32]. A recent

* *Corresponding author:* Fax: +1 519 7464979.
E-mail address: zhwchen@uwaterloo.ca (Z. Chen).
0008-6223/$ - see front matter
doi:10.1016/j.carbon.2010.04.038

study carried out by Gong et al. demonstrated the synthesis of N-CNTs from the pyrolysis of iron (II) phthalocyanine in the presence of ammonia gas. The N-CNTs synthesized showed superior ORR activities compared to platinum based catalysts in alkaline conditions [33]. The ORR activities of N-CNTs have been attributed to the formation of transition metal-nitrogen groups (FeN_4) [34,35], or to the formation of surface nitrogen in the form of pyridinic and pyrrolic/pyridone-type nitrogen groups [36,37]. Despite the differences in active site structures, heavy emphasis was placed on the nitrogen content, where improvements to ORR activities of N-CNTs could be achieved through an increase in nitrogen content. Due to the influence of nitrogen content on the ORR activities of N-CNTs, the relationship between ORR activity and nitrogen content must be elucidated. Although ample studies investigated the effect nitrogen content on the N-CNTs morphology and microstructures [38,39], a systematic study on the direct effect of nitrogen content on ORR activities has not been reported.

In this paper the impact of nitrogen content on the ORR activities of N-CNTs is investigated. The synthesis of N-CNTs was carried out by a single step CVD technique using a solution containing pyridine, ethanol and ferrocene. Through changing the pyridine to ethanol ratios of the stock solution, the relative amount of nitrogen in the growth environment during synthesis can be controlled. This approach allowed the direct comparison of the ORR activities of N-CNTs possessing different nitrogen contents. The morphologies and microstructures of the synthesized N-CNTs were studied using scanning electron microscopy (SEM) and transmission electron microscopy (TEM). X-ray photoelectron microscopy (XPS) and rotating ring disc electrode (RRDE) voltammetry was used for the characterization of surface nitrogen group concentration and ORR activities respectively.

2. Experimental methods

2.1. Synthesis of N-CNTs

A CVD setup with a Lindberg Blue horizontal tube furnace and an injection pump was utilized for N-CNTs synthesis. A stock solution consisted of pyridine (99%, Caledon Laboratory Chemicals), ethanol (HPLC grade, Aldrich) and ferrocene (98%, Aldrich) was used in the synthesis. The stock solution was prepared by mixing pyridine with ethanol at different ratios and dissolving ferrocene at 2.5 wt.% concentration in the mixture. Pyridine to ethanol ratios of the stock solution was varied to create a difference in the total nitrogen content in the stock solution. Pyridine to ethanol ratios of 1:0 (no ethanol), 2:1 and 1:1 were used. The N-CNTs synthesized from these stock solutions will be denoted as N-CNT-a, N-CNT-b and N-CNT-c, respectively throughout this paper. For each synthesis, 3 mL of stock solution was injected into the tube furnace by an injection pump. The reaction was carried out at 800 °C for 1 h with a N_2 flow of 95 sccm under atmosphere condition. The substrates used in the synthesis were pieces of small quartz tube (100 mm length, 18 mm O.D.), placed in the centre of the tube furnace during the reaction. After the reaction at 800 °C, the furnace temperature was held at 400 °C and air was allowed into the furnace. After the furnace was cooled down to room temperature, N-CNTs were collected from the soot deposited on the inner surface of the quartz tube. The obtained products were treated in 0.5 M of sulphuric acid for 5 h and dried overnight in a vacuum oven.

2.2. Physicochemical characterization

Scanning electron microscopy (LEO FESEM 1530) was used to investigate the morphology of N-CNTs. Transmission electron microscopy (PHILIPS CM300) was used to examine the microstructures on the surface of N-CNTs. X-ray photoelectron spectroscopy (XPS) (Thermal Scientific K-Alpha XPS spectrometer) was used to investigate the surface nitrogen group and chemical composition of the N-CNTs.

2.3. Electrocatalytic evaluation

The electrocatalytic activity of the N-CNT samples was measured using RRDE voltammetry. The RRDE voltammetry setup consisted of an AFCBP-1 biopotentiostat (Pine Instrument Co.) and an AFMSRCE rotation speed controller (Pine Instrument Co.). The RRDE has a collection efficiency of 0.26 and it consists of a glassy carbon electrode (5 mm in diameter) and a platinum ring. The sample for RRDE voltammetry was an ink solution containing 4 mg of N-CNTs suspended in 2 mL of 0.2 wt.% Nafion solution. The ink solution was sonicated to ensure good dispersion of the N-CNTs. For each RRDE voltammetry experiment, a uniform film covering the glassy carbon area of the working electrode was formed by depositing 20 μL of ink onto the working electrode. The working electrode was immersed into a glass cell containing 0.1 M of potassium hydroxide together with a double junction Ag/AgCl reference electrode and a counter electrode made from a platinum wire encased in glass tube. Prior to each RRDE voltammetry experiment, the electrolyte was saturated with oxygen. During the RRDE voltammetry, the potential of the working electrode was swept from −0.5 V to 0.2 V at a rate of 10 mV/s while the ring potential was held at 0.5 V. The RRDE voltammetry was performed for different working electrode rotation speed, and the background to each RRDE voltammetry was performed in nitrogen saturated electrolyte with no rotation.

3. Results and discussion

3.1. SEM, TEM and EDX analysis

SEM images of the N-CNTs samples are shown in Fig. 1. The SEM images showed similar morphology of the N-CNTs samples with high degree of alignment. However, increase in diameter is observed with N-CNTs sample with lower nitrogen content similar to results from the literatures [40,41]. From Fig. 2, TEM analysis carried out on the N-CNT-a sample illustrates the formation of bamboo structures, a common feature found in N-CNTs [42,43]. The formation of bamboo-like compartments is caused by the presence of pentagon structures in the graphite network due to nitrogen doping [44]. Additionally, surface defects in the form of graphite plane edges are clearly visible from Fig. 2, resulting from the

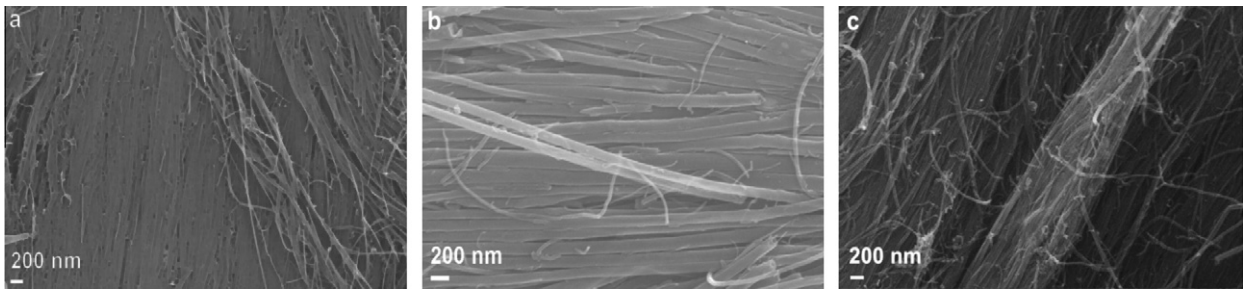

Fig. 1 – SEM images of N-CNTs synthesized with pyridine to ethanol ration of (a) 1:0, (b) 2:1 and (c) 1:1.

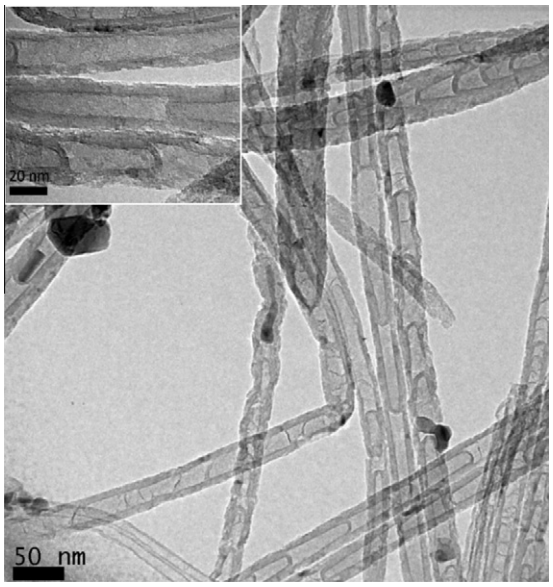

Fig. 2 – TEM images of N-CNT-a.

Table 1 – Elemental composition N-CNTs samples synthesized from different stock solution after acid leaching from EDX.

Composition	N-CNT-a (at.%)	N-CNT-b (at.%)	N-CNT-c (at.%)
Carbon	92.75	92.34	88.57
Nitrogen	3.28	2.84	2.51
Oxygen	3.96	3.92	8.20
Iron	N/A	N/A	0.72

incorporation of nitrogen atoms. Energy dispersive X-ray spectroscopy (EDX) was used to investigate the elemental compositions of the N-CNTs samples. From EDX analysis, the elemental compositions from highest to lowest in N-CNTs samples is carbon, oxygen, nitrogen and iron. The presence of oxygen is owing to the sample exposure to air after growth at 400 °C for the purpose of amorphous carbon removal. The residual iron catalyst after acid treatment contributed to the iron detected by EDX. Results from EDX analysis are summarized in Table 1. A more detailed analysis on the surface elemental compositions of the N-CNTs samples using XPS analysis will be presented later in this paper.

3.2. *RRDE voltammetry analysis*

The electrocatalytic activities of N-CNTs were evaluated by the RRDE voltammetry in alkaline conditions. Higher disc current density and lower ring current density are observed in Fig. 3 for samples with higher nitrogen content. A summary of the ORR performance indicators is showed in Table 2. The half wave potential and limiting current density were obtained from the polarization curves. The number of electrons transferred and H_2O selectivity were calculated using the below equations.

$$n_{e^-} = \frac{4I_D}{I_D + \frac{I_R}{N}} \quad (1)$$

$$\text{Selectivity}_{H_2O} = \left(\frac{I_D - \frac{I_R}{N}}{I_D + \frac{I_R}{N}}\right) * 100 \quad (2)$$

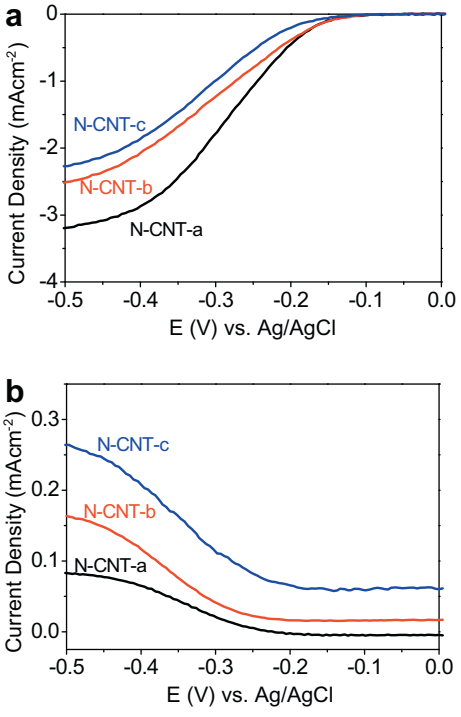

Fig. 3 – Polarization curve of N-CNT-a, N-CNT-b and N-CNT-c samples for oxygen reduction in 0.1 M of potassium hydroxide saturated with O_2. (a) Disk currents and (b) ring currents. Scan rate 10 mV/s and rotation rate 2500 rpm.

Table 2 – Summary of the important ORR performance indicators. Higher ORR performances were observed for higher nitrogen content N-CNTs samples.

	Half wave potential (V)	Limiting current density (mA cm^{-2}, at 2500 rpm)	No. of electrons transferred (at 2500 rpm, −0.5 V)	H_2O selectivity (%, at 2500 rpm, −0.5 V)
N-CNT-a	−0.29	−3.19	3.63	81.82
N-CNT-b	−0.30	−2.52	3.20	59.88
N-CNT-c	−0.31	−2.26	2.76	38.16

In Eqs. (1) and (2), I_D, I_R and N are the disc current, ring current and collection coefficient number, respectively. In general, an improvement to ORR performance is observed as nitrogen content in N-CNTs samples increases based on the data presented in Table 2. However, only minor improvements on half wave potential (~0.01 V) is observed for N-CNTs samples with higher nitrogen content. Additionally, the onset of the reduction reaction does not vary much with an increase in nitrogen content. These minor improvements of onset and half wave potentials can be explained by the slight increase in nitrogen content between the samples. For example, comparing N-CNT-b to N-CNT-a, only 0.44 at.% difference in nitrogen content was observed (based on Table 1). The ORR performance observed by RRDE voltammetry was correlated to the nitrogen content of the N-CNTs. Nitrogen can exist in carbon nanotube as dopant atoms by forming chemical bonds to the carbon atoms or it could be encapsulated as nitrogen gas in the bamboo-like compartments [45]. However the trapped nitrogen gas does not greatly impact the ORR due to two factors. First, when nitrogen gas is trapped in the bamboo-like compartment it does not interact with the reaction environment. Secondly, given that the trapped nitrogen gas managed to escape from the compartments, based on the electrochemistry of ORR, nitrogen atom does not play a role in the electrochemcial reaction. Furthermore, before performing RRDE voltammetry using oxygen, baseline of the experiment was collected using nitrogen gas saturated electrolyte. Thus, any effect from the nitrogen gas was thus removed from the ORR data that was used to carry out the analysis. Owing to these reasons, the trapped nitrogen gas was not considered when correlating the nitrogen content with ORR performance of N-CNTs.

In terms of H_2O selectivity, significant improvement from 38.16% (N-CNT-c) to 81.82% (N-CNT-a) is observed. H_2O selectivity provides information on the reduction mechanisms the molecular oxygen follows during the electrochemical reaction. As proposed by Yeager et al., ORR can occur through a four electron pathway where molecular oxygen is reduced to form H_2O or, a two electron pathway where molecular oxygen is reduced to hydrogen peroxide – an intermediate that will be further reduced to form H_2O [46]. Both reaction pathways in alkaline condition are showed below.

Four electron pathway:

$$O_2 + H_2O + 4e^- \rightarrow 4OH^-$$

Two electron pathway:

$$O_2 + H_2O + 2e^- \rightarrow HO_2^- + OH^-$$
$$HO_2^- + H_2O + 2e^- \rightarrow 3OH^-$$

Consequently, a higher H_2O selectivity value is an indication of the more efficient four electron pathway being the dominant reaction mechanism during the electrochemical reaction. For conventional carbon electrodes in acidic and alkaline conditions, the ORR generally follows the two electron pathway [47]. Based on the observed H_2O selectivity values, the N-CNT-c sample containing the lowest nitrogen content behaved in this manner with the two electron pathway being the dominant mechanism during ORR. On the contrary, ORR followed the four electron pathway for the N-CNT-a sample containing the highest nitrogen content.

In terms of limiting current density, a higher value was obtained with higher nitrogen concentration. In particular, the limiting current density of N-CNT-a increased 41% compared with N-CNT-c for a only a small increment in nitrogen content. This result suggests that N-CNT-a sample contains more active sites for ORR compared with N-CNT-c. Such a conclusion is expected as nitrogen containing sites have been considered as active sites for ORR, thus higher nitrogen content can be correlated with higher limiting current densities. Based on the analysis of limiting current density and H_2O selectivity, significant improvements to these parameters suggests that nitrogen doping has a significant effect in influencing the ORR reaction pathway and catalytically active sites. On the contrary, minor improvements to onset and half wave potentials suggest a minimal influence of nitrogen doping on ORR in the kinetically limited regime.

ORR performance of the N-CNTs catalysts in the diffusion and kinetically limited regime can be evaluated using Koutecky–Levich (KL) plots. The KL plot which presents a linear relationship between the reciprocal of measured current density (j), kinetic current density (j_k), and the reciprocal of the square root of rotation speed (ω) as shown below

$$\frac{1}{|j|} = \frac{1}{|j_k|} + \frac{1}{B\sqrt{\omega}} \quad (3)$$

with B being the Levich slope which can be further defined as,

$$B = 0.62 * n * FC_{O_2} D_{O_2}^{\frac{2}{3}} V^{-\frac{1}{6}} \quad (4)$$

where n is the number of electrons transferred, F is the Faraday constant, C_{O_2} is the bulk oxygen concentration, D_{O_2} is the diffusion coefficient of oxygen and V is the kinematic viscosity of the solution. Fig. 4 shows the KL plots and polarization curves of N-CNTs catalysts at different potentials and rotation speeds respectively. Based on Fig. 4, a linear relationship is observed for $1/j$ and $\omega^{-1/2}$. In addition, for all N-CNT samples the Levich slope showed minor variations at applied potentials, which is an indication of first order kinetics of ORR [48,49]. By extrapolation of the linear KL lines to the origin of the plot, or as ω approaches ∞, the Y-intercept yields the kinetic current density. The kinetic current densities of different N-CNTs samples at various potentials are tabulated in Table 3 where higher kinetic current density is observed for higher nitrogen content samples.

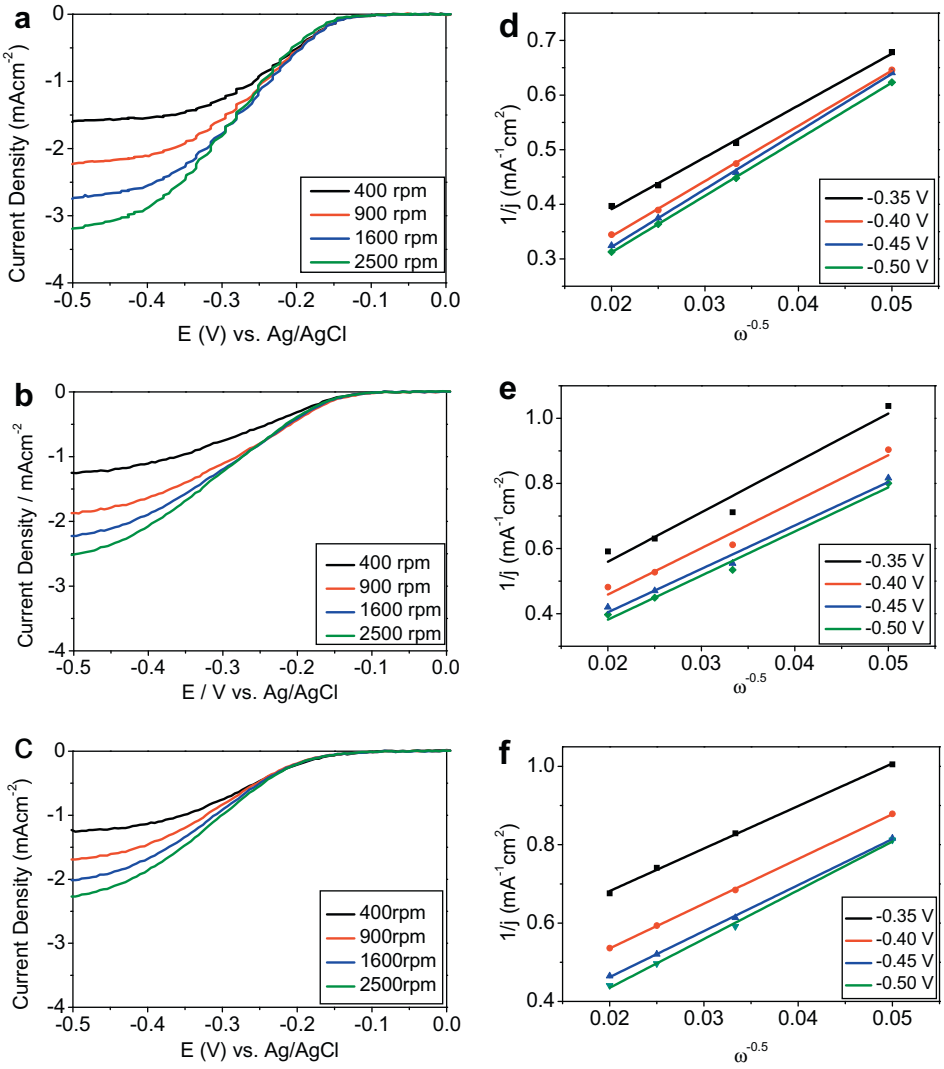

Fig. 4 – Polarization curve of (a) N-CNT-a, (b) N-CNT-b, (c) N-CNT-c for oxygen reduction in 0.1 M of potassium hydroxide saturated with O_2, and Koutecky–Levich plot of (d) N-CNT-a, (e) N-CNT-b and (f) N-CNT-c.

Tafel analysis can be used to evaluate the ORR kinetics and adsorption mechanisms of oxygen on the N-CNTs catalysts. By plotting the applied potential versus the logarithm of measured current density, a Tafel plot can be generated. The linear regions in the Tafel plot can be modelled by the empirical Tafel equation as shown below.

$$\eta = a + b * \log|j| \quad (5)$$

where η is the overpotential, j is the measured current density, b is the Tafel slope and a is a constant. The Tafel plots of different N-CNT samples are showed in Fig. 5. Two distinct linear regions are displayed in the Tafel plots in the low and high current density regions. The double Tafel slope is often observed for platinum based electrocatalysts where the value of these Tafel slopes at low and high current density is −0.06 V per decade and −0.12 V per decade, respectively [50,51]. The Tafel slopes of N-CNT-a are close to that of platinum based catalysts whereas the Tafel slopes of N-CNT-b and N-CNT-c showed greater values. Since a lower value of Tafel slope is desirable, high Tafel slope values indicate inferior ORR activities. Within the three N-CNT samples, N-CNT-a, with the highest nitrogen content showed the smallest Tafel slopes indicating positive impacts of nitrogen content on ORR kinetics, consistent with analysis from the previous sections. From the Tafel plots, by extrapolation of the linear Tafel relationships to zero potential, the X-intercept obtained is the exchange current density. Owing to the negative sloping nature of Tafel slopes, a higher Tafel slope would generate a lower exchange current density. Hence for N-CNTs samples, N-CNT-a having the highest nitrogen content will have the highest exchange current density.

Table 3 – Kinetic current density of different N-CNTs samples at various potentials.

Potential E (V) vs. Ag/AgCl	N-CNT-a j_k (mA cm^{-2})	N-CNT-b j_k (mA cm^{-2})	N-CNT-c j_k (mA cm^{-2})
−0.35	4.97	3.90	2.15
−0.40	7.19	5.77	3.26
−0.45	9.04	7.27	4.40
−0.50	9.53	9.02	5.37

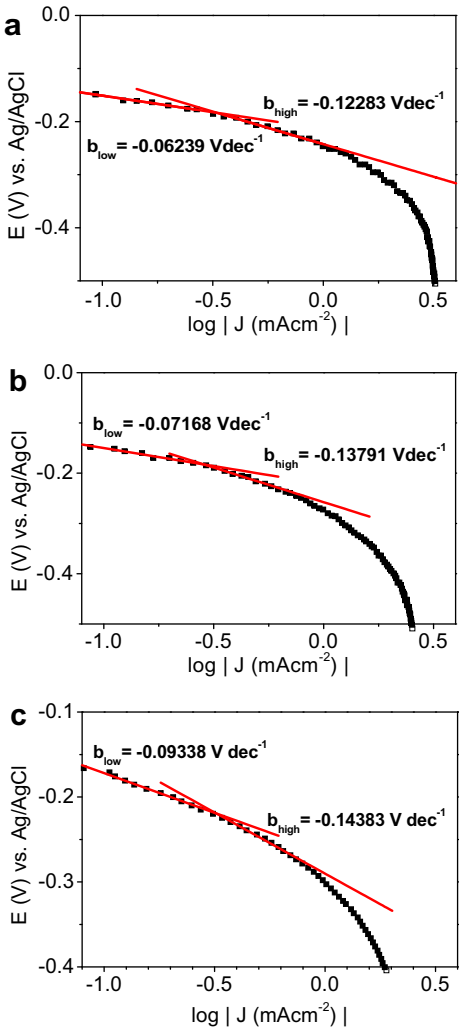

Fig. 5 – Tafel plot of (a) N-CNT-a, (b) N-CNT-b and (c) N-CNT-c.

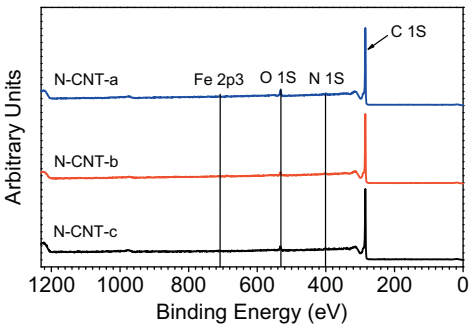

Fig. 6 – XPS spectrum of N-CNTs samples.

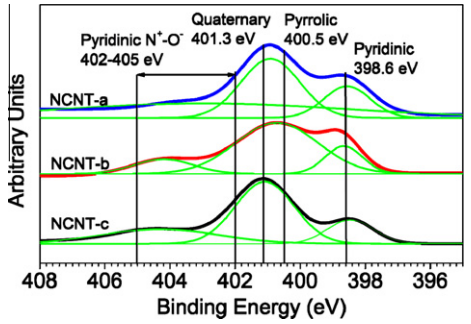

Fig. 7 – High resolution XPS analysis of N1s signals of N-CNT samples.

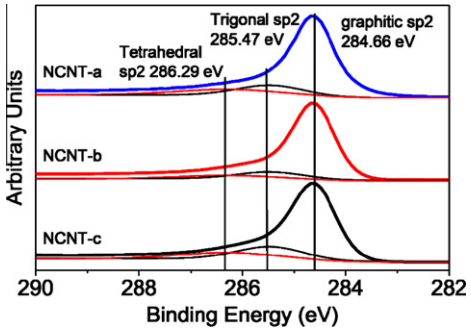

Fig. 8 – Detailed XPS analysis of C1s signals of N-CNT samples.

In terms of the oxygen adsorption mechanism, molecular oxygen adsorbs onto the oxide containing platinum surfaces following the Temkin adsorption isotherm in the low current density region, whereas in the high current density region, molecular oxygen adsorbs onto the pure platinum surface following the Langmuir adsorption isotherm [50,51]. The existence of two Tafel slopes for N-CNTs samples indicates the existence of similar oxygen adsorption mechanism compared to platinum based catalysts.

3.3. *XPS analysis*

ORR typically occurs on the surface active sites of catalysts, thus understanding the distribution of surface nitrogen atoms and the bond formation with carbon atoms of the graphite network is critical. The surface nitrogen groups were identified with XPS due to the high surface sensitivity of the catalyst materials. XPS analysis of N-CNTs samples is shown in Figs. 6–8. A summary of elemental composition of N-CNTs sample is shown in Table 4 where N-CNT-a displayed higher nitrogen content compared to the other two N-CNT samples. The trend of increasing nitrogen content with respect to increasing nitrogen precursor proportion in the stock solution was expected as a higher nitrogen precursor proportion creates a nitrogen rich environment during synthesis. From the work of Bulusheva et al., solution mixtures of toluene and acetonitrile at different proportions were used for the growth of N-CNTs. The nitrogen content of the resultant N-CNTs has increased from 1.23 at.% to 2.89 at.% when the acetonitrile proportion in the solution mixture increased from 25% to 100% [52]. Other literatures have used NH_3 gas as a source of nitrogen dopant and the nitrogen composition of reaction environment was controlled by the fraction of NH_3 gas in feed gas during synthesis. Using varying NH_3 gas fraction, Maldonado et al. has successfully synthesized N-CNTs and observed a linear increase in the nitrogen content with increasing fraction of NH_3 gas in feed gas [53]. Interestingly, based on the study carried out by Ayala et al., nitrogen

Table 4 – Elemental compositions of N-CNTs samples from XPS analysis.

	N-CNT-a		N-CNT-b		N-CNT-c	
	Peak position (eV)	At. %	Peak position (eV)	At. %	Peak position (eV)	At. %
Carbon	284.61	92.70	284.68	95.04	284.66	97.06
Nitrogen	400.41	2.35	400.94	1.27	400.59	0.70
Oxygen	532.40	4.75	532.70	3.61	532.09	2.21
Iron	707.39	0.20	707.34	0.08	708.20	0.04

content in the N-CNT reached a maximum value despite further increase in the nitrogen composition during synthesis [54]. The different trends observed could be cause by the different nitrogen precursors used or the reaction conditions, such as the reaction temperature. Hence, the trend observed in this experiment agrees with some reported literatures, where higher nitrogen content in the N-CNTs could be correlated with higher nitrogen proportion in the growth environment. However, for different systems this correlation between nitrogen content in the N-CNT and nitrogen composition in synthesis environment can change, and more detail study regarding this correlation is definitely needed.

The formation of different surface nitrogen groups was revealed by detail analysis of the N1s spectra. Table 5 summarized the peak position of different types of surface nitrogen group and corresponding contributions to the total surface nitrogen content. The quaternary/pyrrolic nitrogen group with binding energy of 400.7 eV (N-CNT-a and N-CNT-b) and 401.1 eV (N-CNT-c) constituted greater than 65% of the total N1s signals is considered the dominant surface nitrogen group. The preferred formation of quaternary/pyrrolic nitrogen groups at low nitrogen content is commonly observed in literature [40,41]. In close proximity the binding energy of pyrrolic and quaternary nitrogen groups at 400.5 eV and 401.3 eV, respectively, forms a peak, which suggests the coexistence of pyrrolic and quaternary nitrogen groups. However, pyrrolic nitrogen groups are considered the dominant nitrogen group for N-CNT-a and N-CNT-b as the corresponding N1s signal at 400.75 eV and 400.74 eV is in closer proximity to the binding energy of pyrrolic nitrogen groups. Similarly, quaternary nitrogen groups are considered the dominant nitrogen group for N-CNT-c as the corresponding N1s signal at 410.3 eV is in closer proximity to the binding energy of quaternary nitrogen groups. Through coupling the XPS and RRDE results, N-CNT-a and N-CNT-b containing more pyrrolic nitrogen groups showed better ORR performance compared to N-CNT-c sample containing more quaternary nitrogen groups. The observed correlation of ORR activities with respect to nitrogen groups could be explained by the theory regarding the edge plane nitrogen groups (pyrrolic or pyridinic) being the active site for ORR due to the lone pair electrons [53].

Pyridinic nitrogen with a binding energy of 398 eV constitutes less than 20% of the total N1s signal which agrees with reported results regarding unfavourable formation of pyridinic nitrogen at low nitrogen concentration [40,55]. When a nitrogen atom is added to the graphite network, it disrupts the normal bonding configuration between carbon atoms and there is an energy barrier associated with the energy cost of adding additional nitrogen atoms to the graphite network. This energy cost is realized in the form of heat of formation which shows an increasing trend with respect to overall nitrogen content until it reaches a high nitrogen content after which it decreases drastically. This is trend is observed for corrugated graphite network, which is closely related to the pyridinic nitrogen group formation. As a result, the pyridinic nitrogen group exhibits low heat of formation at higher nitrogen content, which explains its more favourable formation at higher nitrogen content [55].

According to the literature, N1s signals around 404 eV can be attributed to pyridone N^{+}–O^{-} groups which are formed when oxygen is present during the pyrolysis of nitrogen containing carbon materials [56,57]. In this experiment, the reaction between oxygen and nitrogen during growth is possible as the synthesis was carried out in ambient pressure. The primary oxygen source in N-CNT-a is from the air, since there is no oxygen in the molecular structure of pyridine. However for the sample N-CNT-b and N-CNT-c, ethanol was mixed with pyridine thus the oxygen atoms from ethanol decomposition could contribute to the presence of oxygen being observed in the EDX and XPS data of N-CNT-b and N-CNT-c samples.

From the XPS analysis, the C1s signal centred at 284.66 ± 0.02 eV is close to the sp2 hybridized graphitic carbon at 284.3 eV [53]. The discrepancy between the observe C1s signal and the perfect sp2 hybridized graphitic carbon is in the forms of a 0.3 eV shift in the peak position and peak asymmetry. The observed peak shift and asymmetric peak shape has been attributed to the disorder of the graphitic network. One source of such disorder could be the nitrogen dopant atoms in

Table 5 – Detail breakdown of N1s signal showing the peak position and relative composition of different surface nitrogen groups.

	N-CNT-a		N-CNT-b		N-CNT-c	
	Peak position (eV)	At. %	Peak position (eV)	At. %	Peak position (eV)	At. %
Quaternary/pyrrolic	400.75	68.20	400.74	66.28	401.12	65.94
Pyridinic	398.47	14.83	398.70	17.69	398.42	17.41
Pyridone	404.87	16.96	404.20	16.02	404.49	16.65

the graphitic network. Another cause of the peak shift and peak asymmetry could be the core–hole screening phenomenon of metallic or high conductive N-CNTs [53]. To confirm the role of nitrogen induced disorder in peak asymmetry, the side peaks at 285.6 eV and 286.7 eV need to be observed. The peaks at 285.6 eV and 286.7 eV correspond to the sp2 and sp3 hybridized bonding geometry between nitrogen and carbon [38]. However, based on the C1s signal from XPS results, the side peaks cannot be distinctively resolved from the main peak. Owing to the ambiguity of the nature of the asymmetric peak, C1s signal is not considered to be the best evidence in supporting nitrogen doping into the carbon nanotubes.

4. Conclusion

N-CNTs with different nitrogen content were obtained by changing the proportion of nitrogen precursor in the stock solution. Based on RRDE voltammetry studies, higher nitrogen content of the resultant N-CNTs was showed to be important for the improvement of ORR activities. While a small increase in nitrogen content does not greatly affect the onset and half wave potentials of the ORR, higher nitrogen content was showed to have significant impact on the limiting current density and H_2O selectivity. In conclusion, employing different nitrogen feed ratios of the source solution influences the nitrogen contents in N-CNTs which is important in attaining high ORR activities.

Acknowledgements

This work was financially supported by the National Sciences and Engineering Research Council of Canada (NSERC) and the University of Waterloo.

REFERENCE

[1] Zhang L, Zhang JJ, Wilkinson DP, Wang HJ. Progress in preparation of non-noble electrocatalysts for PEM fuel cell reactions. J Power Sources 2006;156(2):171–82.
[2] Arico AS, Bruce P, Scrosati B, Tarascon JM, Van Schalkwijk W. Nanostructured materials for advanced energy conversion and storage devices. Nat Mater 2005;4(5):366–77.
[3] Bauen A, Hart D. Assessment of the environmental benefits of transport and stationary fuel cells. J Power Sources 2000;86(1–2):482–94.
[4] Luo C, Zuo XL, Wang L, Wang EG, Song SP, Wang J, et al. Flexible carbon nanotube–polymer composite films with high conductivity and superhydrophobicity made by solution process. Nano Lett 2008;8(12):4454–8.
[5] Sreekumar TV, Liu T, Min BG, Guo H, Kumar S, Hauge RH, et al. Polyacrylonitrile single-walled carbon nanotube composite fibers. Adv Mater 2004;16(1):58–61.
[6] Chen YS, Huang JH, Chuang CC. Glucose biosensor based on multiwalled carbon nanotubes grown directly on Si. Carbon 2009;47(13):3106–12.
[7] Castro M, Lu JB, Bruzaud S, Kumar B, Feller JF. Carbon nanotubes/poly(epsilon-caprolactone) composite vapour sensors. Carbon 2009;47(8):1930–42.
[8] Hoa ND, Van Quy N, Kim D. Nanowire structured SnOx–SWNT composites: high performance sensor for NOx detection. Sens Actuators B 2009;142(1):253–9.
[9] Maghsoodi S, Gholami Z, Chourchian H, Mortazavi Y, Khodadadi AA. A novel biosensor using entangled carbon nanotubes layer grown on an alumina substrate by CCVD of methane on FeOx–MgO. Sens Actuators B 2009;141(2):526–31.
[10] Huang JR, Wang JH, Gu CP, Yu K, Meng FL, Liu JH. A novel highly sensitive gas ionization sensor for ammonia detection. Sens Actuators A 2009;150(2):218–23.
[11] Arranz-Andres J, Blau WJ. Enhanced device performance using different carbon nanotube types in polymer photovoltaic devices. Carbon 2008;46(15):2067–75.
[12] Hino T, Ogawa Y, Kuramoto N. Dye-sensitized solar cell with single-walled carbon nanotube thin film prepared by an electrolytic micelle disruption method as the counterelectrode. Fullerenes Nanotubes Carbon Nanostruct 2006;14(4):607–19.
[13] Frackowiak E, Beguin F. Electrochemical storage of energy in carbon nanotubes and nanostructured carbons. Carbon 2002;40(10):1775–87.
[14] Fraysse J, Minett AI, Jaschinski O, Duesberg GS, Roth S. Carbon nanotubes acting like actuators. Carbon 2002;40(10):1735–9.
[15] Frackowiak E, Beguin F. Carbon materials for the electrochemical storage of energy in capacitors. Carbon 2001;39(6):937–50.
[16] Baughman RH, Zakhidov AA, de Heer WA. Carbon nanotubes – the route toward applications. Science 2002;297(5582):787–92.
[17] Bianco A, Kostarelos K, Prato M. Applications of carbon nanotubes in drug delivery. Curr Opin Chem Biol 2005;9(6):674–9.
[18] Dalton AB, Collins S, Munoz E, Razal JM, Ebron VH, Ferraris JP, et al. Super-tough carbon-nanotube fibres – these extraordinary composite fibres can be woven into electronic textiles. Nature 2003;423(6941):703.
[19] Ding L, Tselev A, Wang JY, Yuan DN, Chu HB, McNicholas TP, et al. Selective growth of well-aligned semiconducting single-walled carbon nanotubes. Nano Lett 2009;9(2):800–5.
[20] Postma HWC, Teepen T, Yao Z, Grifoni M, Dekker C. Carbon nanotube single-electron transistors at room temperature. Science 2001;293(5527):76–9.
[21] Wang MY, Chen JH, Fan Z, Tang H, Deng GH, He DL, et al. Ethanol electro-oxidation with Pt and Pt-Ru catalysts supported on carbon nanotubes. Carbon 2004;42(15):3257–60.
[22] Tang H, Chen JH, Huang ZP, Wang DZ, Ren ZF, Nie LH, et al. High dispersion and electrocatalytic properties of platinum on well-aligned carbon nanotube arrays. Carbon 2004;42(1):191–7.
[23] Britto PJ, Santhanam KSV, Rubio A, Alonso JA, Ajayan PM. Improved charge transfer at carbon nanotube electrodes. Adv Mater 1999;11(2):154–7.
[24] Lefevre M, Dodelet JP. Fe-based catalysts for the reduction of oxygen in polymer electrolyte membrane fuel cell conditions: determination of the amount of peroxide released during electroreduction and its influence on the stability of the catalysts. Electrochim Acta 2003;48(19):2749–60.
[25] Lalande G, Cote R, Guay D, Dodelet JP, Weng LT, Bertrand P. Is nitrogen important in the formulation of Fe-based catalysts for oxygen reduction in solid polymer fuel cells? Electrochim Acta 1997;42(9):1379–88.
[26] Strelko VV, Kartel NT, Dukhno IN, Kuts VS, Clarkson RB, Odintsov BM. Mechanism of reductive oxygen adsorption on active carbons with various surface chemistry. Surf Sci 2004;548(1–3):281–90.
[27] Strelko VV, Kuts VS, Thrower PA. On the mechanism of possible influence of heteroatoms of nitrogen, boron and

phosphorus in a carbon matrix on the catalytic activity of carbons in electron transfer reactions. Carbon 2000;38(10):1499–503.
[28] Wei G, Wainright JS, Savinell RF. Catalytic activity for oxygen reduction reaction of catalysts consisting of carbon, nitrogen and cobalt. J New Mater Electrochem Syst 2000;3(2):121–9.
[29] Ledoux MJ, Vieira R, Pham-Huu C, Keller N. New catalytic phenomena on nanostructured (fibers and tubes) catalysts. J Catal 2003;216(1–2):333–42.
[30] Matter PH, Wang E, Arias M, Biddinger EJ, Ozkan US. Oxygen reduction reaction activity and surface properties of nanostructured nitrogen-containing carbon. J Mol Catal A 2007;264(1–2):73–81.
[31] Shao YY, Sui JH, Yin GP, Gao YZ. Nitrogen-doped carbon nanostructures and their composites as catalytic materials for proton exchange membrane fuel cell. Appl Catal B 2008;79(1–2):89–99.
[32] Maldonado S, Stevenson KJ. Influence of nitrogen doping on oxygen reduction electrocatalysis at carbon nanofiber electrodes. J Phys Chem B 2005;109(10):4707–16.
[33] Gong KP, Du F, Xia ZH, Durstock M, Dai LM. Nitrogen-doped carbon nanotube arrays with high electrocatalytic activity for oxygen reduction. Science 2009;323(5915):760–4.
[34] Lefevre M, Dodelet JP, Bertrand P. Molecular oxygen reduction in PEM fuel cells: evidence for the simultaneous presence of two active sites in Fe-based catalysts. J Phys Chem B 2002;106(34):8705–13.
[35] Yang JB, Liu DJ, Kariuki NN, Chen LX. Aligned carbon nanotubes with built-in FeN4 active sites for electrocatalytic reduction of oxygen. Chem Commun 2008;(3):329–31.
[36] Matter PH, Wang E, Arias M, Biddinger EJ, Ozkan US. Oxygen reduction reaction catalysts prepared from acetonitrile pyrolysis over alumina-supported metal particles. J Phys Chem B 2006;110(37):18374–84.
[37] Maldonado S, Stevenson KJ. Direct preparation of carbon nanofiber electrodes via pyrolysis of iron(II) phthalocyanine: electrocatalytic aspects for oxygen reduction. J Phys Chem B 2004;108(31):11375–83.
[38] Chun KY, Lee HS, Lee CJ. Nitrogen doping effects on the structure behavior and the field emission performance of double-walled carbon nanotubes. Carbon 2009;47(1):169–77.
[39] Lin YG, Hsu YK, Wu CT, Chen SY, Chen KH, Chen LC. Effects of nitrogen-doping on the microstructure, bonding and electrochemical activity of carbon nanotubes. Diamond Relat Mater 2009;18(2–3):433–7.
[40] Terrones M, Terrones H, Grobert N, Hsu WK, Zhu YQ, Hare JP, et al. Efficient route to large arrays of CNx nanofibers by pyrolysis of ferrocene/melamine mixtures. Appl Phys Lett 1999;75(25):3932–4.
[41] Terrones M, Redlich P, Grobert N, Trasobares S, Hsu WK, Terrones H, et al. Carbon nitride nanocomposites: formation of aligned CxNy nanofibers. Adv Mater 1999;11(8):655–8.
[42] Sumpter BG, Meunier V, Romo-Herrera JM, Cruz-Silva E, Cullen DA, Terrones H, et al. Nitrogen-mediated carbon nanotube growth: diameter reduction, metallicity, bundle dispersability, and bamboo-like structure formation. Acs Nano 2007;1(4):369–75.
[43] Jang JW, Lee CE, Lyu SC, Lee TJ, Lee CJ. Structural study of nitrogen-doping effects in bamboo-shaped multiwalled carbon nanotubes. Appl Phys Lett 2004;84(15):2877–9.
[44] Sumpter BG, Huang JS, Meunier V, Romo-Herrera JM, Cruz-Silva E, Terrones H, et al. A theoretical and experimental study on manipulating the structure and properties of carbon nanotubes using substitutional dopants. Int J Quantum Chem 2009;109(1):97–118.
[45] Reyes-Reyes M, Grobert N, Kamalakaran R, Seeger T, Golberg D, Ruhle M, et al. Efficient encapsulation of gaseous nitrogen inside carbon nanotubes with bamboo-like structure using aerosol thermolysis. Chem Phys Lett 2004;396(1–3):167–73.
[46] Yeager E. Dioxygen electrocatalysis – mechanisms in relation to catalyst structure. J Mol Catal 1986;38(1–2):5–25.
[47] Sidik RA, Anderson AB, Subramanian NP, Kumaraguru SP, Popov BN. O_2 reduction on graphite and nitrogen-doped graphite: experiment and theory. J Phys Chem B 2006;110(4):1787–93.
[48] Gochi-Ponce Y, Alonso-Nunez G, Alonso-Vante N. Synthesis and electrochemical characterization of a novel platinum chalcogenide electrocatalyst with an enhanced tolerance to methanol in the oxygen reduction reaction. Electrochem Commun 2006;8(9):1487–91.
[49] Pattabi M, Castellanos RH, Castillo R, Ocampo AL, Moreira J, Sebastian PJ, et al. Electrochemical characterization of tungsten carbonyl compound for oxygen reduction reaction. Int J Hydrogen Energy 2001;26(2):171–4.
[50] Wakabayashi N, Takeichi M, Itagaki M, Uchida H, Watanabe M. Temperature-dependence of oxygen reduction activity at a platinum electrode in an acidic electrolyte solution investigated with a channel flow double electrode. J Electroanal Chem 2005;574(2):339–46.
[51] Halseid R, Bystron T, Tunold R. Oxygen reduction on platinum in aqueous sulphuric acid in the presence of ammonium. Electrochim Acta 2006;51(13):2737–42.
[52] Bulusheva LG, Okotrub AV, Kinloch IA, Asanov IP, Kurenya AG, Kudashov AG, et al. Effect of nitrogen doping on Raman spectra of multi-walled carbon nanotubes. Phys Status Solidi B 2008;245(10):1971–4.
[53] Maldonado S, Morin S, Stevenson KJ. Structure, composition, and chemical reactivity of carbon nanotubes by selective nitrogen doping. Carbon 2006;44(8):1429–37.
[54] Ayala P, Grüneis A, Kramberger C, Rummeli MH, Solorzano IG, Freire FL, Jr et al. Effects of the reaction atmosphere composition on the synthesis of single and mulitwalled nitrogen-doped nanotubes. J Chem Phys 2007;127(8):184709-1–6.
[55] dos Santos MC, Alvarez F. Nitrogen substitution of carbon in graphite: structure evolution toward molecular forms. Phys Rev B 1998;58(20):13918–24.
[56] Stanczyk K, Dziembaj R, Piwowarska Z, Witkowski S. Transformation of nitrogen structures in carbonization of model compounds determined by XPS. Carbon 1995;33(10):1383–92.
[57] Pels JR, Kapteijn F, Moulijn JA, Zhu Q, Thomas KM. Evolution of nitrogen functionalities in carbonaceous materials during pyrolysis. Carbon 1995;33(11):1641–53.